PHYSICAL REVIEW B **71**, 125424 (2005)

Accuracy and resolution limits of Kelvin probe force microscopy

Ulrich Zerweck, Christian Loppacher,* Tobias Otto, Stefan Grafström, and Lukas M. Eng
Institute of Applied Photophysics, University of Technology Dresden, D-01062 Dresden, Germany

(Received 28 October 2004; published 25 March 2005)

Kelvin probe force microscopy is a scanning probe technique capable of mapping the local surface potential or work function on various surfaces with high spatial resolution. This technique can be realized on the basis of either an amplitude-sensitive method or a frequency-modulation method, which are sensitive to the electrostatic force and its gradient, respectively. We present a detailed experimental and theoretical study of the accuracy and resolution provided by the two methods, including the setup for the frequency-modulation technique. Au(111) with a submonolayer coverage of KCl serves as a test sample exhibiting extended sharply bounded areas that differ in work function by an amount well known from ultraviolet photoelectron spectroscopy. The influence of all relevant experimental parameters on the measurement is investigated. The experimental results are compared with the predictions of a numerical simulation based on a realistic model for the tip-sample geometry. Good agreement is found. The experimental analysis allows us to specify the lateral, vertical, and potential resolution that can be achieved with the two methods for a given tip size. Our work clearly proves that the frequency-modulation method is preferable in most applications because it (i) provides much higher lateral resolution, (ii) yields quantitative surface potential values on areas larger than the tip radius, and (iii) is little affected by variations of the tip-sample distance during topographic imaging.

DOI: 10.1103/PhysRevB.71.125424 PACS number(s): 68.37.Ps, 73.30.+y

I. INTRODUCTION

Since the invention of atomic force microscopy[1] (AFM) many different operation modes and setups have been developed for AFM investigations of specific physical properties with a spatial resolution in the nanometer range. In particular, noncontact AFM (NC-AFM),[2,3] in which the force-sensing cantilever is vibrated at its resonance frequency at a small tip-sample separation, has become very popular within the last couple of years, not only because it allows a nondestructive measurement of topography, but also because it achieves atomic contrast even on insulators and single molecules[4,5] with an image quality similar to scanning tunneling microscopy (STM).[6] However, the forces acting between the AFM tip and the surface under inspection are much more complicated to understand than the tunneling current in STM. Besides the short-range forces which decay on a similar length scale as the tunneling current,[7–11] long-range forces such as van der Waals and electrostatic forces can strongly influence topographic imaging. In particular the electrostatic forces play a major role for many applications. These forces, on the one hand, may dominate the interaction and even lead to inverted topography contrast, for example on heterogeneous samples with spatial variations of the local work function.[12] On the other hand, long-ranged electrostatic forces contain important physical information about the electronic properties of the sample surface.

Kelvin probe force microscopy (KPFM) is a NC-AFM operation mode in which the electrostatic interaction is minimized by application of an appropriate bias voltage during topographic imaging.[13,14] For metals this voltage corresponds to the local work function difference between sample and tip [contact potential difference (CPD)], whereas for insulators it gives information about the surface charge. The use of KPFM offers the advantage that not only the true topography is recorded,[12] but also a map of the surface potential distribution is acquired.[15] To date, KPFM has been used to measure local dopant concentrations,[16,17] surface charging due to photoinduced charge separation,[18–20] interface dipole layers formed between a metal surface and an organic[21,22] or ionic thin film,[23] electronic band bending at semiconducting interfaces,[24–29] local material contrast on different facets of a nanocrystal,[30] at grain boundaries,[31] and on ordered and disordered surfaces,[32] to name only a few examples. In a few experiments, even molecular[33] or atomic contrast[34] has been reported. These examples show that the chemical contrast provided by KPFM reveals important information in addition to the sample surface topography.

Various methods for implementing KPFM have been proposed so far. In electric force microscopy (EFM), for example, the tip is scanned at a constant height above the sample surface. At large distances (>10 nm), the long-range electrostatic forces dominate and can be measured independently from topography.[35] However, the method suffers not only from an increased recording time (topographic and EFM images cannot be acquired simultaneously) but also from a reduced lateral resolution due to the large tip-sample separation.

In this work, we concentrate on methods by which the electrostatic interaction is recorded simultaneously to topographic imaging. These methods can be divided into two groups.

(i) The amplitude-sensitive method (AM-KPFM), in which an additional ac voltage excites a mechanical oscillation of the cantilever.[13] AM-KPFM has been implemented in different variants, which all have their advantages and disadvantages, as discussed in more detail later. Common to all of them is that they minimize the electrostatic force by nullifying the mechanical oscillation amplitude.

(ii) The frequency-modulation method (FM-KPFM) detects the resonance frequency shift Δf induced by the bias voltage applied between tip and sample. This method is quite well established for single-point measurements.[36] In this case, the parabolic dependence of Δf on the bias voltage is recorded $[\Delta f(U)$ parabola$]$ and used to evaluate the CPD between tip and sample. Kitamura and Iwatsuki [37] modified this method to simultaneously measure CPD and topography. FM-KPFM is sensitive to the force gradient,[3] which is much more confined to the tip front end than the force. Hence, for the FM method we expect a higher lateral resolution than for the force-sensitive AM method.

In the following, we present results obtained with both methods on well-defined samples with extended areas of different surface potential, measured with tips of known geometry, widely varying spring constants, and different coatings. These results are analyzed in detail regarding the dependence on all relevant experimental parameters. Results of a numerical simulation are set in relation to the experimental data, and allow us to extrapolate our findings to any tip size and to specify the lateral, vertical, and CPD resolution to be expected for a certain tip.

II. PHYSICAL BACKGROUND OF KPFM

A. Electrostatic force

For both AM- and FM-KPFM, an ac voltage with frequency f_{mod} and amplitude U_{mod}, superimposed on a dc voltage U_{dc}, is applied between tip and sample. The resulting oscillating electrostatic force F_{el} is given by

$$F_{el} = \frac{1}{2}\frac{\partial C}{\partial z}U^2 \text{ with}$$

$$U = U_{\mathrm{dc}} - \frac{\Delta\phi}{e} + U_{mod}\cos(2\pi f_{mod}t). \tag{1}$$

$\Delta\phi$ is the CPD between tip and sample. The capacitance gradient $\partial C/\partial z$ depends on the tip geometry and the tip-sample separation z. Hudlet *et al.*[38] calculated the electrostatic force for a realistic tip model consisting of a truncated cone that ends in a spherical cap of radius R. For a simple estimation, we can neglect the contribution of the cone and apply the formula for a charged sphere at a separation z above an infinite plane:[38]

$$F_{el}(z) = -\pi\varepsilon_0\left(\frac{R^2}{z(z+R)}\right)U^2. \tag{2}$$

Calculating the force for $U=100$ mV, $R=15$ nm, and $z=3$ nm yields an electrostatic force $F_{el}=-1.2\times10^{-12}$ N, which produces a deflection $\Delta b=F_{el}/k=-1.2$ pm for a spring constant $k=1$ N/m of the cantilever. This deflection is far below the noise limit of most detection units.

Equation (1) can be separated into three different terms as follows:

$$F_{el} = \frac{1}{2}\left[\left(U_{\mathrm{dc}} - \frac{\Delta\phi}{e}\right)^2 + \frac{1}{2}U_{mod}^2\right]\frac{\partial C}{\partial z} \tag{3}$$

$$+ \frac{\partial C}{\partial z}\left(U_{\mathrm{dc}} - \frac{\Delta\phi}{e}\right)U_{mod}\cos(2\pi f_{mod}t) \tag{4}$$

$$+ \frac{1}{4}\frac{\partial C}{\partial z}U_{mod}^2\cos(2\times2\pi f_{mod}t). \tag{5}$$

According to Eqs. (3)–(5) the electrostatic force consists of a static part and two contributions at f_{mod} and $2f_{mod}$. As mentioned above, the static part is difficult to detect, whereas the dynamic part at f_{mod} can accurately be detected with a lock-in amplifier (LIA) in order to determine the CPD $\Delta\phi$.

B. Amplitude modulation

In AM-KPFM (Ref. 39) the electrostatic force oscillating with f_{mod} is measured by direct detection of the lever deflection by means of a LIA referenced to f_{mod}. For determining the CPD, a feedback loop tunes the detected amplitude to zero by adjusting U_{dc} to $\Delta\phi/e$ [see Eq. (4)]. For a constant modulation voltage U_{mod}, the $2f_{mod}$ component [Eq. (5)] only depends on the capacitance gradient and, therefore, can be used for measurements of the local capacitance or the dielectric constant of the sample.[40]

Phase-sensitive detection of the mechanical oscillation amplitude at f_{mod} with a LIA already leads to a major improvement compared to detecting the static part of F_{el}. However, this method still requires soft cantilevers ($\sim$3 N/m) with low resonance frequencies ($\sim$70 kHz) and large modulation amplitudes in order to obtain a sufficiently large and detectable mechanical deflection. One can achieve a larger deflection, however, by using the first overtone f_1 of the cantilever to induce the mechanical oscillation by adjusting $f_{mod}\approx f_1$. Compared to off-resonance modulation, the sensitivity is increased by the quality factor Q_1 of the resonance, which under UHV conditions can reach values up to 10^5. It is thus possible to excite the oscillation with a small voltage. This is of major importance for semiconducting samples for which voltages exceeding 100 mV may lead to asymmetric bias-induced band bending.[32] However, detection of the mechanical oscillation at f_1 suffers from a long settling time, $\tau_1=Q_1/f_1$, which drastically reduces the permissible scan speed. Furthermore, the limited bandwidth of most detection electronics allows excitation of the first overtone $f_1=6.28\times f_0$ only for soft cantilevers, which have a resonance frequency f_0 of typically less than 100 kHz.

C. Frequency modulation

An external long-range force with gradient $\partial F/\partial z$ changes the fundamental mechanical resonance frequency $f_0=1/2\pi\times\sqrt{k/m^*}$ of a cantilever with an effective mass m^* as follows:

$$f_0' = \frac{1}{2\pi}\sqrt{\frac{k-\partial F/\partial z}{m^*}} \approx f_0\left(1-\frac{1}{2k}\frac{\partial F}{\partial z}\right). \tag{6}$$

All long-range forces including the electrostatic force F_{el} shift the resonance frequency according to Eq. (6). The applied ac voltage modulates F_{el} and with it $\partial F_{el}/\partial z$ according to Eqs. (4) and (5). Hence, as follows from Eq. (6), the mechanical resonance of the cantilever is frequency modulated with frequencies f_{mod} and $2f_{mod}$. Figure 1 shows a schematic frequency spectrum of the cantilever oscillation. Be-

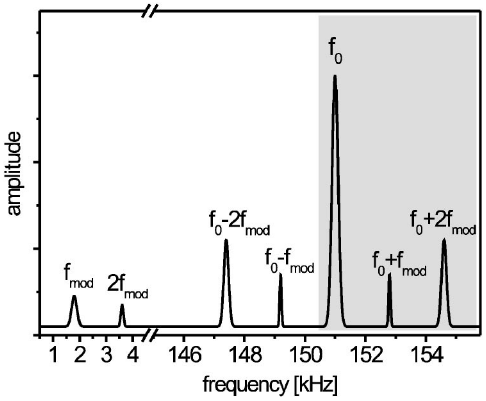

FIG. 1. Schematic frequency spectrum of the tip oscillation. The peaks at f_{mod} and $2f_{mod}$ originate from the electrostatic force, whereas the peaks at $f_0 \pm f_{mod}$ and $f_0 \pm 2f_{mod}$ show the frequency modulation of f_0, produced by the oscillating electrostatic force gradient. The experimental spectrum for the gray-shaded frequency range is depicted in Fig. 2.

sides peaks at f_{mod} and $2f_{mod}$ resulting directly from the force modulation, sidebands appear at $f_0 \pm f_{mod}$ and $f_0 \pm 2f_{mod}$ adjacent to the fundamental resonance peak at f_0. These sidebands originate from the modulated force gradient. FM-KPFM nullifies the signal at $f_0 \pm f_{mod}$ by applying an appropriate bias voltage U_{dc}. This again yields $U_{dc}=\Delta\phi/e$.

The real spectrum, obtained with our instrument under UHV conditions, is shown in Fig. 2. Only the gray-shaded frequency range (see Fig. 1) between f_0 and f_0+2f_{mod} is displayed and shows the amplitudes at f_0+f_{mod} and f_0+2f_{mod} for $U_{dc}-\Delta\phi/e=1000$ mV (black), 50 mV (dark gray), and 5 mV (light gray). Even at a potential difference as small as 5 mV the sideband at f_0+f_{mod} is still well resolved. Hence, the CPD can be determined with an accuracy clearly better than 5 mV. With increasing $U_{dc}-\Delta\phi/e$ the f_0+f_{mod} peak rises, whereas the f_0+2f_{mod} peak maintains a constant height, as expected from Eq. (3) since $\partial C/\partial z$ for a given distance is constant.

Contrary to AM-KPFM, FM-KPFM does not rely on soft cantilevers, but allows using stiff cantilevers with spring constants in the range of several tens of N/m. The decreased sensitivity of hard cantilevers is partially compensated by the possibility to approach closer to the surface where the force gradient is larger. Furthermore, stiff cantilevers provide more stable topographic imaging.

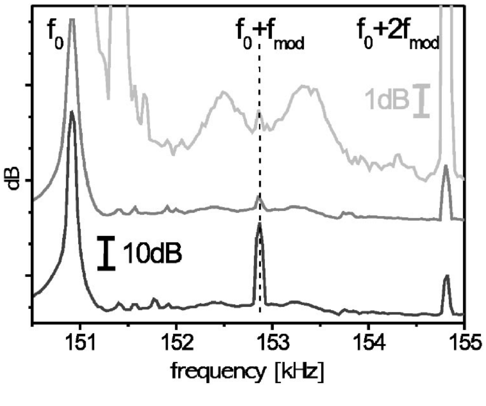

FIG. 2. Experimental frequency spectra showing the spectral lines at f_0, $f_0 \pm f_{mod}$, and $f_0 \pm 2f_{mod}$. The three curves were measured at different bias voltages corresponding to an uncompensated contact potential difference of 1000 mV (black), 50 mV (dark gray), and 5 mV (light gray, y scale 10 times enlarged).

III. METHODS

A. Sample preparation

In an earlier work[23] we investigated the work function change of the Au(111) surface after deposition of an ultrathin dielectric layer of alkali-metal chloride with a coverage of less than a monolayer (ML). That work reported the CPD $\Delta\phi$ to depend linearly on the radius of the alkali ion. When evaporating half a monolayer of KCl on Au(111), we observed a carpetlike growth of the film, which formed closed islands laterally extending over several micrometers and frequently decorated by smaller rectangular islands in the second monolayer. We chose these samples as ideal test structure for the KPFM studies reported here because they (a) are easy to prepare in a reproducible way, (b) show large, homogeneous areas of Au(111) and KCl-covered Au(111) with sharp boundaries, and (c) exhibit a rather large work function difference between bare and KCl-covered regions.

Preparation and measurement were throughout performed in ultrahigh vacuum. The gold substrate was cleaned by repeated cycles of sputtering (~37 μA Ar^+ flux at 1 keV for 5 min) and annealing (5 min to 450 °C). The last annealing for 15 min to 400 °C finished the substrate preparation. Half a monolayer of KCl was evaporated from a homebuilt crucible onto the Au(111) surface at a rate of 1 ML/min. The evaporation was performed during cooldown of the crystal in order to provide a high surface mobility of the KCl molecules, allowing the formation of large, closed islands.

B. Experimental setup

FM- and AM-KPFM was performed with a commercial cryogenic UHV STM/AFM system[41] using the SCALA software and electronics for scanning and data acquisition. The digital NC-AFM controller is a homebuilt phase-stabilized electronics[42] consisting of a digital amplitude feedback controller maintaining a constant tip oscillation independent of the tip-surface interaction, and a digital phase-locked loop (PLL) used to keep the frequency shift Δf constant by controlling the tip-sample distance. The use of a PLL ensures a constant phase angle between the detected cantilever oscillation and its excitation which is of great importance for KPFM when phase-sensitive lock-in techniques are implemented.

Figure 3 displays a block diagram of our setup. The deflection signal of the cantilever is fed to the digital NC-AFM electronics, which contain both the amplitude and the frequency shift controller. The KPFM part contains two lock-in amplifiers (LIA-1 and LIA-2). The internal reference of LIA-2 is used for the bias voltage modulation for both AM- and FM-KPFM. Note that the frequency bandwidth of the NC-AFM electronics is set much lower than f_{mod}, resulting

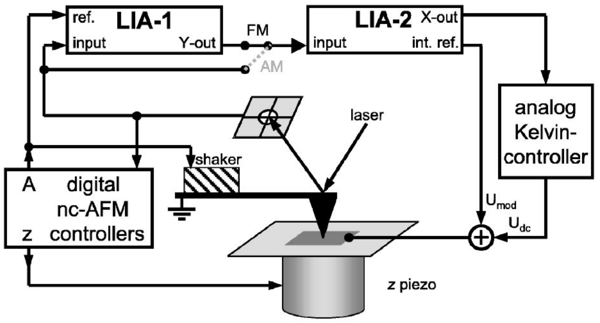

FIG. 3. Block diagram of the FM-KPFM setup. The cantilever oscillation signal is fed to the digital NC-AFM electronics which controls the oscillation amplitude A and the tip-sample distance z. For FM-KPFM feedback the signal passes through two lock-in amplifiers (LIAs) and is then fed back to the analog Kelvin controller. For AM-KPFM, LIA-1 is omitted.

in topographic imaging that is not affected by the electrostatic frequency modulation.

For FM-KPFM, the deflection signal is fed into LIA-1 whose external reference is the cantilever excitation signal with frequency f_0, which is also applied to the shaker piezo. LIA-1 is used as a mixer with adjustable phase rather than as a phase-sensitive rectifier. The purpose of LIA-1 is to FM-demodulate the sidebands at $f_0 \pm f_{mod}$.

The frequency-modulated lever deflection signal d can be written as

$$d = A_0 \sin\left(2\pi f_0 t + \varphi + \frac{\delta f}{f_{mod}} \sin(2\pi f_{mod} t)\right), \qquad (7)$$

where A_0 is the oscillation amplitude and φ is a constant phase. δf denotes the amplitude of the frequency modulation. For $\delta f \ll f_{mod}$ Eq. (7) can be recast in the following form:

$$d = A_0 \sin(2\pi f_0 t + \varphi) + A_0 \frac{\delta f}{f_{mod}} \sin(2\pi f_{mod} t) \cos(2\pi f_0 t + \varphi). \qquad (8)$$

The first term on the right-hand side is the carrier, whereas the second term represents the sidebands at $f_0 \pm f_{mod}$. The latter term constitutes an oscillation that is phase shifted by 90° with respect to the carrier and whose amplitude oscillates with the modulation frequency f_{mod}. With a proper setting of the phase at LIA-1, the constant carrier amplitude A_0 appears at the X output of the LIA, while the demodulated FM signal is available at the Y output as an ac signal with frequency f_{mod}. This signal is further demodulated by LIA-2, which provides a dc signal proportional to $\partial^2 C/\partial z^2 (U_{dc} - \Delta\phi/e)$ [see Eq. (4)]. This voltage serves as input error signal for the analog Kelvin feedback controller, which nullifies the error by applying an appropriate voltage $U_{dc} = \Delta\phi/e$ between tip and sample.[43] For AM-KPFM, the cantilever deflection signal is directly connected to LIA-2. In this way, the tip oscillation amplitude at the modulation frequency f_{mod} is measured (f_{mod} is a few kilohertz only and, hence, far off resonance in our experiments). Processing of the LIA-2 output signal is the same as for FM-KPFM.

The speed of the KPFM feedback was tested by modulating the setpoint with a rectangular signal and simultaneously recording the controller response. Noise analysis was performed by recording the U_{dc} output. From these measurements, we determined a bandwidth of our FM-KPFM feedback of ≈35 Hz and a noise level of 19 mV (standard deviation). However, averaging the KPFM signal over a larger sample area as shown for example in Fig. 4 or limiting the bandwidth of the KPFM feedback reduces the noise level and provides a CPD resolution better than 5 mV (see Fig. 2).

C. Modeling KPFM

So far, calculations of the electrostatic interaction between tip and sample have mostly been performed for the electrostatic force F_{el}.[44–46] For FM-KPFM, however, the force gradient $\partial F_{el}/\partial z$ is decisive. In a purely theoretical work, Colchero *et al.*[47] calculated $\partial F_{el}/\partial z$ for different tip and sample potentials and estimated a lateral resolution. However, these authors assumed a homogeneous surface potential and did not calculate the tip potential for minimized interaction. This prohibits a direct comparison with the experiment. We performed numerical simulations of the electrostatic interaction between tip and sample. The tip is modeled as a truncated cone with an opening angle α merging into a half sphere with radius R opposed to a circular surface with diameter D representing the sample. The cantilever is described as a large disk with the same diameter at the base of the cone. Disk, cone, and half sphere (representing cantilever and tip) are set to the same potential in accordance with the experiment.

We considered two different cases. (i) A three-dimensional (3D) model with $D = 20\ \mu$m was used to analyze the lateral resolution at a boundary between two regions of different surface potential. The sample was split into two halves with the left and right parts being at negative and positive potential, respectively. A smooth transition of the potential between the two halves was introduced at large distances from the tip. This drastically reduces computing time. (ii) To analyze the problem of different tip radii and of varying object size, the sample was modeled as a circular disk at 1 V potential surrounded by a grounded area. As the problem becomes rotationally symmetric in this case, we could speed up computing by calculating the two-dimensional profile only which allowed us to increase the diameter to $D = 30\ \mu$m.

The electric field distribution $\mathbf{E}(\mathbf{r}, z, U)$ for different separations z and potential differences U between tip and sample was calculated in a cylindrical volume with diameter D and height $z + 10\ \mu$m (corresponding to the separation z plus the tip height of 10 μm). The electric field energy $W(z, U)$ was obtained by integration of $|\mathbf{E}(\mathbf{r}, z, U)|^2$ over the whole volume of the cylinder. $W(z, U)$ was differentiated to get the electrostatic force $F_{el}(z, U)$ acting along the surface normal and its gradient $\partial F_{el}(z, U)/\partial z$ with respect to the separation z:

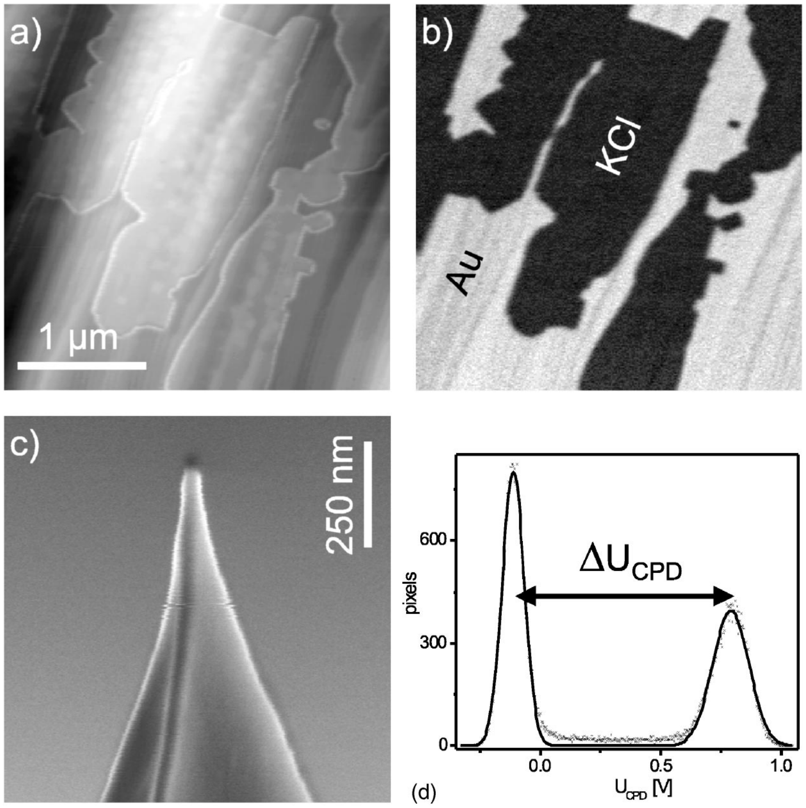

FIG. 4. Half a monolayer of KCl on Au(111). (a) The topography shows large areas covered by 1 ML of KCl with rectangular KCl islands in the second monolayer (gray scale 3.4 nm). (b) Simultaneously recorded CPD (FM-KPFM). Note that the second monolayer of KCl does not further change the CPD contrast (gray scale −0.32 to 0.93 V). (c) SEM image of the Pt/Ir-coated tip after the experiment. The tip radius measures 17 nm. (d) Histogram belonging to (b) fitted with two Gaussian peaks. The peak separation is $\Delta U_{CPD}=909$ mV.

$$F_{el}(z,U) = \frac{\partial W(z,U)}{\partial z} \quad \text{and}$$

$$\frac{\partial F_{el}(z,U)}{\partial z} = \frac{\partial^2 W(z,U)}{\partial z^2}. \tag{9}$$

For a fixed separation and lateral position, both $F_{el}(z,U)$ and $\partial F_{el}(z,U)/\partial z$ depend on U via $W(z,U)$. The CPD provided by the two KPFM methods corresponds to the minimum of either F_{el} (AM-KPFM) or $\partial F_{el}/\partial z$ (FM-KPFM) with respect to U. These voltages were determined numerically.

IV. POTASSIUM CHLORIDE ON Au(111)

A typical NC-AFM image of KCl at a submonolayer coverage on clean Au(111) is depicted in Fig. 4. The topography [Fig. 4(a)] shows atomically flat gold terraces covered with an incomplete first monolayer of KCl and small rectangular islands in the second monolayer. The FM-KPFM signal in Fig. 4(b) is the U_{dc} output stemming from the Kelvin controller (see Fig. 3). The second monolayer of KCl does not further change the CPD, from which we conclude that the interface dipole is confined to the first monolayer. The curve displayed in Fig. 4(d) shows a histogram calculated from the CPD values in Fig. 4(b). The curve shows two Gaussian-shaped peaks, the separation of which corresponds to the work function difference between Au(111) and KCl-covered Au(111). A Gaussian fit to the data reveals a peak separation of $\Delta U_{CPD}=909$ mV. The error of the fitted peak positions is in the order of only 1 mV. However, measurements performed with different tips yielded results that differed by several tens of mV.

In order to deduce the influence of the tip on the acquired CPD we compared results obtained with three cantilevers of different geometry and spring constant:[48] A force-modulation-type cantilever ($k=1.7$ N/m, $f_0=69$ kHz) and two noncontact-type cantilevers with different geometries ($k=24.1$ N/m, $f_0=151$ kHz and $k=23.2$ N/m, $f_0=290$ kHz). We found that neither k nor f_0 has any influence on the value of the detected CPD in the case of FM-KPFM. Furthermore, we compared highly n-doped silicon tips (with native oxide) with tips from which the oxide had been removed by *in situ* Ar^+ sputtering, as well as with metallized tips (Pt/Ir coated). The measured ΔU_{CPD} values were 949, 917, and 909 mV, respectively. The slightly higher ΔU_{CPD} obtained with the oxide-covered cantilever might indicate charge accumulation at the tip. However, the highly conducting sputtered and metallized tips yielded the same ΔU_{CPD} within 1%. Thus, we are confident that these values obtained by FM-KPFM are quantitative and reliable values.

Figure 4(c) additionally shows the scanning electron microscopy (SEM) image of the Pt/Ir-coated AFM tip after the experiment. Such a SEM analysis is important both for proving the nondestructiveness of our method and to deduce the tip radius, as needed for modeling. The tip radius measures 17 nm perfectly agreeing with the manufacturer's data sheet. In all experiments, we took great care not to destroy the tip or the Pt/Ir coating, because especially metallized tips were found to yield an unstable KPFM signal if the coating had been damaged.[49]

To further underline the quantitative correctness of the CPD values determined above, the KCl/Au(111) sample was inspected by ultraviolet photoelectron spectroscopy (UPS). Figure 5 shows an UPS spectrum of the pure Au(111) sub-

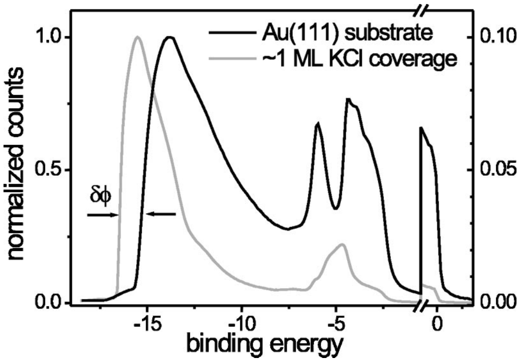

FIG. 5. UPS spectra for bare Au(111) (black) and the Au(111) surface covered with a closed layer of KCl (gray). Evaluation of the onset energy reveals a change of the work function by $\delta\phi = 906$ meV.

strate (black curve) with its characteristic valence band structure. The binding energy is referred to the Fermi edge displayed with an enlarged scale on the right. The work function can be extracted from the onset energy on the left. The gray curve displays the spectrum for the fully KCl-covered substrate. The Fermi edge remains unchanged and the valence band structure of the gold has almost vanished. Evaluation of the onset energy before and after KCl deposition reveals a shift $\delta\phi = 906$ meV in excellent agreement with the FM-KPFM result.

A. Lateral resolution and accuracy

For a direct comparison between the CPD signals obtained with the two different detection methods (i.e., AM- and FM-KPFM), a KCl island boundary was imaged with both methods. Figure 6(a) shows a CPD image in which the upper and lower halves display the FM- and AM-KPFM results, respectively. As seen from the profiles in Fig. 6(b), the signal rise from 10% to 90% appears within a width of 50 nm for FM-KPFM, whereas the AM signal does not saturate even over more than 400 nm. Our experimental finding thus strongly favors FM-KPFM due to its higher lateral resolution.

Figure 6(b) additionally displays the results of our 3D simulation. The tip apex radius R was set to 15 nm and the potential was assumed to change within 2 nm from -0.45 to $+0.45$ V, in accordance to the experiment ($\delta\phi = 906$ meV). To account for the tip vibration, we averaged the derivatives in Eq. (9) over the oscillation. The oscillation amplitude was set to 5 nm with a minimum separation z of 3 nm. At a distance of 25 nm from the potential step, FM-KPFM detects the correct potential values, whereas AM-KPFM is unable to provide the quantitative values within the investigated lateral range.

Our calculations clearly prove that quantitative results are only obtained with the FM method. Because of the larger decay length of F_{el}, the AM method suffers from poor spatial resolution so that quantitative CPD values can only be expected on large homogeneous sample regions. Being sensitive to $\partial F_{el}/\partial z$, FM-KPFM provides much higher lateral resolution and therefore is able to image much smaller features (see Sec. IV E).

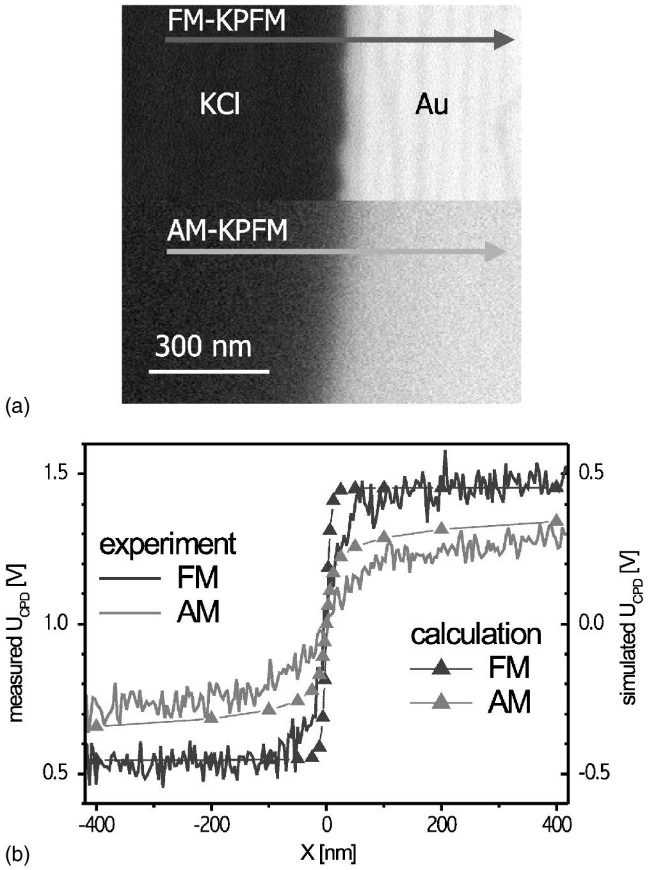

FIG. 6. (a) Kelvin image of a KCl island boundary. The upper part was recorded with FM-KPFM (gray scale 0.36 to 1.61 V) and the lower part with AM-KPFM (gray scale 0.87 to 1.60 V). Line profiles were taken along the arrows and are shown in (b). A larger contrast and a steeper transition of U_{CPD} is obtained with FM- than with AM-KPFM. For the simulation, a potential difference of 0.9 V between the two regions was assumed.

B. Tip-sample distance dependence

When performing KPFM measurements, especially in the AM mode, we observed the contrast of the Kelvin image to vary when the frequency set point was changed corresponding to a change of the tip-sample distance. This, of course, leads to artifacts in the KPFM signal on rough surfaces. In order to understand the distance dependence in more detail, we imaged a boundary of a KCl island by both methods in an xz scan. For this, the tip was positioned 120 nm above the surface and scanned at constant height along the x direction. After each line, the tip was approached toward the sample surface by ≈ 1 nm. The resulting image is displayed in Fig. 7(a).

For each line (each z value) we evaluated the CPD contrast by subtracting the mean values obtained along the right (dark) and left (bright) third of the line from each other, thus neglecting the points close to the boundary where the CPD changes. The contrast as a function of the separation z is

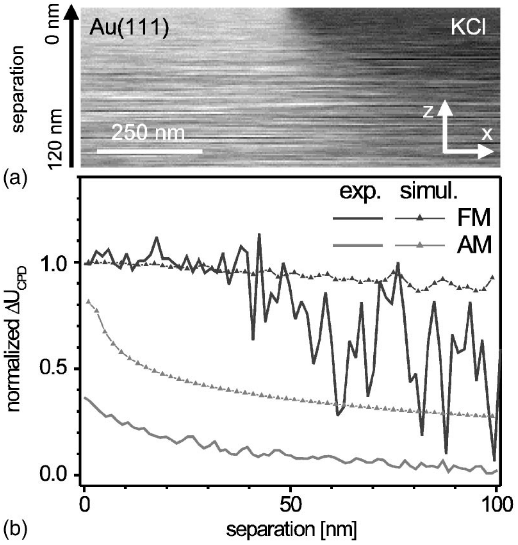

FIG. 7. Distance dependence of ΔU_{CPD} between KCl/Au(111) and Au(111), normalized to the value obtained from UPS data. Exemplarily, the FM-KPFM image of an *xz* scan centered over an island boundary is shown. During the approach, the AM signal rises monotonically without reaching the full contrast. Experimentally, FM-KPFM is unstable for separations $z > 30$ nm but yields the full contrast closer to the surface. Experimental (solid) and simulated curves (scattered) are in good agreement.

depicted in Fig. 7(b). The experimental data (solid curves) were normalized to the value obtained by UPS (see Sec. IV) and are compared with simulated data (scattered).

On the one hand, the AM-KPFM contrast [gray line in Fig. 7(b)] constantly rises until short-range energy dissipation starts and the tip would finally crash into the surface if further approached. Even at such small tip-sample separations, the correct contrast as obtained with UPS is not reproduced. On the other hand, with FM-KPFM [black line in Fig. 7(b)] ΔU_{CPD} provides the correct value for separations as large as ≈30 nm and remains constant when the tip-sample gap is decreased. For distances larger than 30 nm, the Kelvin feedback controller gets unstable because the voltage-induced frequency shift decreases and the apex of the $\Delta f(U)$ parabola becomes shallower and is no longer detectable.

In order to compare our experimental findings with theory, we performed a distant-dependent simulation using the rotationally symmetric two-dimensional model. In these calculations, the tip (compare Sec. III C) was centered above a KCl island of 500 nm radius kept at +1 V potential, with the surrounding area at 0 V. The theoretical AM curves in Fig. 7(b) reproduce well the shape of the experimental curves, although an offset is observed. The latter might either be due to a small offset of the set point of the Kelvin feedback, which can produce large errors when the tip is retracted, or stem from a difference in geometry between simulation and experiment (simulation: circular island and smooth island boundary). The simulated FM approach curve [Fig. 7(b)] matches well the experimental one for distances <30 nm for which the controller is stable.

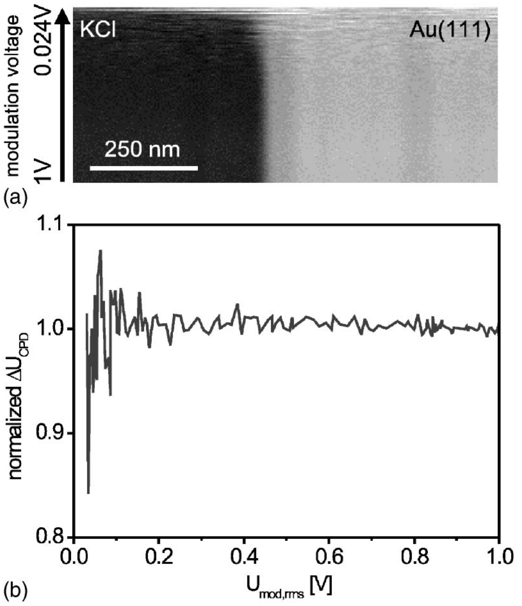

FIG. 8. Observed CPD contrast versus modulation voltage. U_{mod} can be reduced from 1 V (root mean square) down to 100 mV without changing ΔU_{CPD}. For smaller voltages, the feedback becomes unstable.

C. Dependence on mechanical oscillation amplitude

For the FM-KPFM method, the influence of the mechanical oscillation amplitude of the cantilever on the detected ΔU_{CPD} was investigated. ΔU_{CPD} starts to decrease slightly for amplitudes larger than 14 nm, still maintaining ≈97% of its initial value for an amplitude of 24 nm. This dependence can be explained with the distance dependence investigated above: For a peak-peak amplitude larger than 30 nm the tip enters a regime where it becomes impossible to detect the full ΔU_{CPD}. Note that all results presented in this work were recorded with oscillation amplitudes smaller than 10 nm.

D. Dependence on modulation voltage

For the investigation of semiconductors it is of great benefit to avoid any potential difference between tip and sample in order to prevent tip-induced band bending. Although the Kelvin controller minimizes the static electric field, the modulation voltage remains. Therefore, in AM-KPFM, efforts were undertaken to minimize this voltage by taking advantage of the quality factor of the first overtone[27] as mentioned in Sec. II B.

To find the minimum modulation voltage needed for FM-KPFM, we repeatedly scanned the tip across the border of a KCl island while slowly reducing U_{mod}. The recorded CPD is displayed in Fig. 8(a) as a grayscale plot with the vertical axis representing the modulation voltage. The contrast ΔU_{CPD} as a function of U_{mod} was extracted with a procedure similar to the one applied to Fig. 7(a). The result is depicted in Fig. 8(b).

The noise in Fig. 8(b) increases with decreasing modulation voltage. This is due to the fact that the the frequency modulation becomes smaller in amplitude, hence tracing a

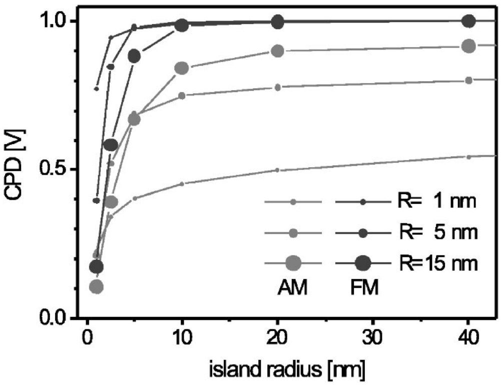

FIG. 9. Theoretical AM- and FM-KPFM signals versus island size for different tip radii. For AM-KPFM, a blunt tip with the same size as the island is preferable. For FM-KPFM, sharp tips are recommended as they sense the exact CPD for islands larger than the tip radius.

much smaller part of the $\Delta f(U)$ parabola. For voltages less than 0.15 $\mathrm{V_{rms}}$ the noise drastically increases and below 0.1 $\mathrm{V_{rms}}$ the Kelvin feedback finally becomes unstable. Imaging closer to the surface reduces the modulation voltage needed for FM-KPFM even more due to the increased curvature of the $\Delta f(U)$ parabola, which provides a larger frequency modulation span. Therefore, with our FM-KPFM setup it is possible to image the CPD with modulation voltages as small as required for semiconducting samples.[27,32] Using such small modulation voltages so far was only possible with the AM method on the first overtone, which however has various disadvantages as mentioned in Sec. II B.

E. KPFM for small objects

As described in Sec. IV A, the lateral resolution of FM-KPFM was found to be ≈50 nm. For objects of a still smaller size, a decreased contrast is expected. In order to quantify the smallest object size still providing a quantitative CPD, we performed additional calculations using our model tip with a reduced tip radius. The island size was varied from 80 nm to 1 nm in radius, hence covering the 50 nm resolution limit of Sec. IV A. The calculated CPD is depicted in Fig. 9 for tip radii of 15 nm, 5 nm, and 1 nm.

The lighter gray curves in Fig. 9 reflect the calculated CPD for AM-KPFM. Far too low CPD values are deduced in AM-KPFM even for large island sizes in the case of sharp tips. This is in good agreement with the conclusion drawn by Jacobs *et al.*[44] that AM-KPFM works best with tips having a small opening angle α and a rather large, blunt end. For small tip radii, the electrostatic force is dominated by the potential sensed by the cone, whereas for larger tip radii the tip end dominates. The potential sensed starts to drop for island sizes smaller than the tip radius.

The black curves in Fig. 9 reveal that FM-KPFM delivers an accurate potential of +1 V for islands larger than the tip radius. When smaller islands are imaged, the tip obviously also senses the 0 V potential surrounding the island and, hence, a reduced CPD is obtained. Unlike in AM-KPFM, where a blunt tip similar in radius to the observed object should be used, sharp tips are recommended in FM-KPFM for any object size.

V. CONCLUSION

We compared two Kelvin probe force microscopy methods with regard to accuracy and resolution: the amplitude-sensitive and the frequency-detection methods. As described in detail, the AM method is sensitive to the electrostatic force F_{el} whereas the FM method is sensitive to its gradient $\partial F_{el}/\partial z$.

Experimentally we used both methods to investigate a KCl-covered Au(111) surface. From ultraviolet photoelectron spectroscopy we could quantitatively deduce a work function difference of 906 mV between pure and KCl-covered gold. At a coverage of half a monolayer, KCl forms micrometer-sized islands with the bare substrate exposed in areas of similar size. Therefore, this was the ideal structure for evaluating KPFM because it presented sharp boundaries between extended areas with a well known difference in surface potential.

Numerical simulations were performed in order to calculate the electrostatic interaction between the tip and the sample. Both tip and sample were modeled to be as close as possible to the experiment. The calculation of F_{el} and its gradient $\partial F_{el}/\partial z$ yielded the contact potential difference that a KPFM controller would deduce when minimizing the corresponding interaction.

For comparison of the two KPFM methods we scanned the tip laterally and vertically across a surface potential boundary and compared the measured CPD with the one obtained from our calculations. We find a good agreement between experiment and simulation. Therefore, we further extended the simulation to small circular islands and calculated the interaction for sharp tips. This allowed us to estimate the lateral resolution limit of both the AM as well as the FM method.

In summary, the most striking results of our work are the following.

(i) The FM method deduces an accurate CPD which is in excellent agreement with macroscopic UPS measurements. This is not the case for the AM method with the tip-sample geometry used in our work.

(ii) The FM method becomes accurate for objects larger than the tip radius. Therefore, the FM method is best used with the sharpest tips and might even achieve atomic contrast with accurate values. For the AM method, reasonable accuracy can only be expected for tips with a front end having a similar size as the object under investigation.

(iii) The FM method does not show any variation of the detected surface potential within a tip-sample separation of 30 nm. However, the AM method exhibits a very strong distance dependence. Therefore, artifacts due to variations in topography can be excluded in FM-KPFM whereas for the AM mode they are very likely to occur.

(iv) Our setup for FM-KPFM works properly for stiff cantilevers, clearly separates topography and Kelvin probe feedback, and allows the use of small modulation voltages which so far was only possible by applying the AM method on the first overtone.

With all these findings we would like to promote the use of the FM method with tips of well known geometry. Only with this method is a quantitative interpretation of KPFM results possible.

ACKNOWLEDGMENT

Financial support by the DFG in the framework of the Projects No. SPP 1136 and No. SFB 287 is gratefully acknowledged.

---

*Corresponding author. Email address: Loppacher@iapp.de

[1] G. Binnig, C. F. Quate, and C. Gerber, Phys. Rev. Lett. **56**, 930 (1986).

[2] Y. Martin, C. Williams, and H. Wickramasinghe, J. Appl. Phys. **61**, 4723 (1987).

[3] T. Albrecht, P. Grütter, D. Horne, and D. Rugar, J. Appl. Phys. **69**, 668 (1991).

[4] F. J. Giessibl, Science **267**, 1451 (1995).

[5] Proceedings of the First International Workshop on Noncontact Atomic Force Microscopy, Osaka, 1998 [Appl. Surf. Sci. **140** (1998)].

[6] G. Binnig and H. Rohrer, Helv. Phys. Acta **55**, 726 (1982).

[7] J. Israelachvili, *Intermolecular and Surface Forces* (Academic Press, London, 1985).

[8] C. Chen, *Introduction to Scanning Tunneling Microscopy* (Oxford University Press, New York, 1993).

[9] U. Dürig and O. Züger, Phys. Rev. B **50**, 5008 (1994).

[10] R. Lüthi, E. Meyer, M. Bammerlin, A. Baratoff, T. Lehmann, L. Howald, C. Gerber, and H.-J. Güntherodt, Z. Phys. B: Condens. Matter **100**, 165 (1996).

[11] C. Loppacher, M. Bammerlin, M. Guggisberg, S. Schär, R. Bennewitz, A. Baratoff, E. Meyer, and H.-J. Güntherodt, Phys. Rev. B **62**, 16 944 (2000).

[12] S. Sadewasser and M. C. Lux-Steiner, Phys. Rev. Lett. **91**, 266101 (2003).

[13] M. Nonnenmacher, M. P. O'Boyle, and H. K. Wickramasinghe, Appl. Phys. Lett. **58**, 2921 (1991).

[14] J. Weaver and D. Abraham, J. Vac. Sci. Technol. B **9**, 1559 (1991).

[15] M. Yasutake, D. Aoki, and M. Fujihira, Thin Solid Films **273**, 279 (1996).

[16] A. K. Henninga, T. Hochwitz, J. Slinkman, J. Never, S. Hoffmann, P. Kaszuba, and C. Daghlian, J. Appl. Phys. **77**, 1888 (1995).

[17] N. Duhayon *et al.*, J. Vac. Sci. Technol. B **22**, 385 (2004).

[18] T. Meoded, R. Shikler, N. Fried, and Y. Rosenwaks, Appl. Phys. Lett. **75**, 2435 (1999).

[19] M. Fujihira, Annu. Rev. Mater. Sci. **29**, 353 (1999).

[20] C. Loppacher, U. Zerweck, S. Teich, E. Beyreuther, T. Otto, S. Grafström, and L. M. Eng, Nanotechnology **16**, S1 (2005).

[21] J. Lü, E. Delamarche, L. Eng, R. Bennewitz, E. Meyer, and H.-J. Güntherodt, Langmuir **15**, 8184 (1999).

[22] H. Sugimura, K. Hayashi, N. Saito, O. Takai, and N. Nakagiri, Jpn. J. Appl. Phys., Part 1 **40**, 4373 (2001).

[23] C. Loppacher, U. Zerweck, and L. M. Eng, Nanotechnology **15**, S9 (2004).

[24] O. Vatel and M. Tanimoto, J. Appl. Phys. **77**, 2358 (1995).

[25] A. Kikukawa, S. Hosaka, and R. Imura, Appl. Phys. Lett. **66**, 3510 (1995).

[26] I. G. Hill, A. Rajagopal, and A. Kahn, Appl. Phys. Lett. **73**, 662 (1998).

[27] C. Sommerhalter, T. Matthes, T. Glatzel, A. Jäger-Waldau, and M. C. Lux-Steiner, Appl. Phys. Lett. **75**, 286 (1999).

[28] R. Shikler, T. Meoded, N. Fried, and Y. Rosenwaks, Appl. Phys. Lett. **74**, 2972 (1999).

[29] T. Glatzel, D. F. Marrón, T. Schedel-Niedrig, S. Sadewasser, and M. C. Lux-Steiner, Appl. Phys. Lett. **81**, 2017 (2002).

[30] S. Sadewasser, T. Glatzel, M. Rusu, A. Jäger-Waldau, and M. Lux-Steiner, Appl. Phys. Lett. **80**, 2979 (2002).

[31] C.-S. Jiang, R. Noufi, J. A. AbuShama, K. Ramanathan, H. R. Moutinho, J. Pankow, and M. M. Al-Jassim, Appl. Phys. Lett. **84**, 3477 (2004).

[32] Y. Leng, C. Williams, L. Suand, and G. Stringfellow, Appl. Phys. Lett. **66**, 1264 (1995).

[33] A. Sasahara, H. Uetsuka, and H. Onishi, Phys. Rev. B **64**, 121406(R) (2001).

[34] Y. Sugawara, T. Uchihashi, M. Abe, and S. Morita, Appl. Surf. Sci. **140**, 371 (1999).

[35] H. O. Jacobs, H. F. Knapp, S. Müller, and A. Stemmer, Ultramicroscopy **69**, 39 (1997).

[36] M. Guggisberg, M. Bammerlin, C. Loppacher, O. Pfeiffer, A. Abdurixit, V. Barvich, R. Bennewitz, A. Baratoff, E. Meyer, and H. J. Güntherodt, Phys. Rev. B **61**, 11 151 (2000).

[37] S. Kitamura and M. Iwatsuki, Appl. Phys. Lett. **72**, 3154 (1998).

[38] S. Hudlet, M. Saint-Jean, C. Guthmann, and J. Berger, Eur. Phys. J. B **2**, 5 (1998).

[39] In AM-KPFM the force is modulated. However, the amplitude is detected and thus the abbreviation AM-KPFM is commonly used.

[40] Y. Martin, D. Abraham, and H. Wickramasinghe, Appl. Phys. Lett. **52**, 1103 (1988).

[41] Omicron NanoTechnology GmbH, Taunusstein, Germany.

[42] C. Loppacher, M. Bammerlin, F. M. Battiston, M. Guggisberg, D. Müller, H. R. Hidber, R. Lüthi, E. Meyer, and H.-J. Güntherodt, Appl. Phys. A: Mater. Sci. Process. **66**, S215 (1998).

[43] The Kelvin controller is an analog proportional-integral (PI) controller built at the University of Basel. We use a Stanford Research SR844 or an EG&G 5302 for LIA-1, and a Stanford Research SR830 for LIA-2. The minimum time constant τ of the output low-pass filter limits the modulation frequency f_{mod} to about 2 kHz for the SR844 and to 15 kHz for the EG&G 5302.

[44] H. O. Jacobs, P. Leuchtmann, O. J. Homann, and A. Stemmer, J. Appl. Phys. **84**, 1168 (1998).

[45] H. McMurray and G. Williams, J. Appl. Phys. **91**, 1673 (2002).

[46] T. Takahashi and S. Ono, Ultramicroscopy **100**, 287 (2004).

[47] J. Colchero, A. Gil, and A. M. Baró, Phys. Rev. B **64**, 245403 (2001).

[48] Levers used are FM-, NC-, and NCL- (long NC-) type cantilevers commercially available from NanoWorld AG, Rue Jaquet-Droz 1, CH-2007 Neuchâtel, Switzerland.

[49] H. Jacobs, H. Knapp, and A. Stemmer, Rev. Sci. Instrum. **70**, 1756 (1999).